Airfoil Lift and Drag in Ideal Conditions

Zakary Steenhoek

This experiment aimed to calibrate a pressure transducer and a scannivalve in a low-speed wind tunnel and to determine the airflow velocity in the test section as a function of fan speed. Calibration curves for the pressure transducer and scannivalve were developed by comparing their digital readings with those from a manometer. Using Bernoulli's equation and mass conservation principles, pressure and velocity relationships were evaluated across a range of fan settings for each instrument. The results show a linear relationship with minimal deviation from the true flow speed. This calibration procedure confirmed the effectiveness of the instruments and laid baseline measurements for an empty test section for future aerodynamic experiments.

I. Nomenclature

ρ	=	air density
$\forbar$	=	volume
n	=	molar mass
R	=	universal gas constant
T	=	temperature
U	=	internal energy
KE	=	kinetic energy
PE	=	potential energy
$C\forbar$	=	control volume
CS	=	control surface
$\hat{n}$	=	normal vector
∂	=	partial derivative
M	=	conversion factor
E	=	voltage
p_{static}	=	static pressure
p_{total}	=	total pressure
p_{gauge}	=	gauge pressure
p_{MM}	=	manometer pressure
V_∞	=	dynamic velocity
$\dot{m}$	=	mass time derivative
A_1	=	upstream cross-sectional area
A_2	=	downstream cross-sectional area
f	=	fan speed
p_1	=	upstream static pressure
p_2	=	downstream static pressure
δP	=	differential pressure across the test section
P_{atm}	=	absolute atmospheric pressure
V_1	=	upstream flow velocity
V_1	=	downstream flow velocity

II. Introduction

Lift and drag across a surface are arguably some of the the most important calculations in aerospace engineering. These values tell the engineer how the surface in question will affect the behavior and design of an aircraft. This process involves measurements of the pressure distribution around the surface exposed to the flow and calculations from those measurements. This process involved two airfoils at various angles of attack and allows the study of the resulting changes in lift and drag. This experiment will use the NACA 0012 and NACA 4412 airfoils.

A. Objective

The goal of this test is first to determine the laboratory air density. This provides an important data point, from which wind-tunnel flow velocity can be determined as a function of pressure. The main objective of this experiment is to determine how a change in the angle of attack of a scaled aircraft airfoil section impacts the resulting lift and drag forces produced. This can be done by first taking pressure measurements through various methods to obtain the pressure coefficient at various locations around the airfoil, and then performing calculations to determine the forces acting. The final objective is to use these measurements to determine lift and drag vs. angle of attack (interchangeably referred to as alpha (α)) slopes. An understanding of how these changes in angle of attack of an airfoil impact the forces produced has a huge impact on aircraft and airfoil design.

B. Assumptions

Assumptions are made in this experiment which make it possible to produce meaningful results without creating substantial error. These assumptions allow for simplicity in data collection and processing, and allow the use of some key physical laws. Assumptions made include the following:

1. Ideal Atmosphere

To determine the density of the laboratory air, the ideal gas law is used, which is only applicable to ideal gasses. The assumption is made that the atmosphere may be be treated as an ideal gas.

2. Incompressible & Uniform Flow

Methods to determine flow velocity through the test area apply the conservation of mass. The fluid flow is assumed to me uniform, and density of laboratory air is assumed to be constant, and therefore the term representing the change in mass inside the control volume w.r.t time evaluates to zero.

3. Inviscid Fluid

Methods to determine flow velocity through the test area apply the conservation of energy. The effects of viscous forces on the fluid are assumed to be negligible, and therefore energy loss can be neglected, and Bernoulli's equation may be applied.

C. Physical Laws

1. Ideal Gas Law

The first governing law in this experiment fundamental ideal gas law, Eq.(1) . This is a thermodynamic equation of state for an ideal gas, which relates physical properties and known constants.

$$p\forall = nRT \tag{1}$$

2. Bernoulli's Equation

The next governing law is the fundamental conservation of energy equation, Eq. (2), which states that the total energy of a system, consisting of the internal energy U, the kinetic energy KE, and the potential energy PE, remains constant.

$$U + KE + PE = const. \tag{2}$$

3. Mass Conservation

The next governing law is the fundamental conservation of mass, Eq.(3), which states that the change in mass inside a control volume w.r.t time plus the mass convected across the control surface must always sum to 0.

$$\frac{\partial}{\partial t}\int_{C\forall} \rho \, d\forall + \int_{CS} \rho(\vec{V}\cdot\hat{n}) \, dA = 0 \tag{3}$$

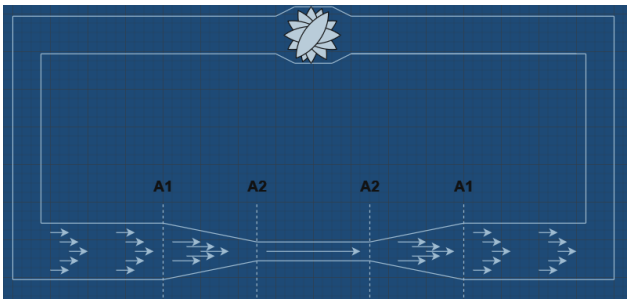

Fig. 1 General wind tunnel setup. Note the contraction area on the left-hand side, where the cross-sectional area reduces from A_1 to A_2.

4. Error Propagation

The final governing equation is Gauss's formula for error propagation, Eq.(4), which describes the effect of uncertainty in a calculation as a function of the uncertainty in the variables involved, where i is the number of variables with uncertainty.

$$\delta y = \sqrt{\sum_i \left(\frac{\partial y}{\partial x_i}\delta x_i\right)^2} \tag{4}$$

D. Experimental Equipment

1. Low-speed wind tunnel

A low speed wind tunnel[1] is a large lab machine with a fan, flow normalization, a test section, and related instrumentation. The tunnel used in this experiment is a closed tunnel, which circulates a constant volume of air through a ducting system using a fan. Before the test section, the cross-sectional area of the tunnel decreases, and according to Eq.(3), the velocity must increase. This closed system creates an optimal environment for aerodynamic testing. A general wind tunnel diagram is shown in Fig.1.

2. NACA 0012 Airfoil

The NACA 0012 airfoil is a standardized airfoil shape defined by the National Advisory Committee for Aeronautics. It is a symmetric airfoil with no camber and a maximum 12% thickness to chord length ratio. The sample NACA 0012 airfoil used here has a chord c of $100mm$.

3. NACA 4412 Airfoil

The NACA 4412 airfoil is a standardized airfoil shape defined by the National Advisory Committee for Aeronautics. It is a non-symmetric airfoil with maximum 4% camber located 40% (0.4 chords) from the leading edge and a maximum 12% thickness to chord length ratio. The sample NACA 0012 airfoil used here has a chord c of $100mm$.

4. Absolute pressure transducer

An absolute pressure transducer[2] is a digital measurement device that measures pressure in the absolute range, i.e. from a zero-reference point, displayed in kilopascals. It works by generating a voltage difference difference between the measurement side, exposed to the atmosphere, and the non-measurement side, which is exposed to a permanently sealed, near-perfect vacuum. This measurement is integral to determining the density of the atmosphere inside of the lab.

5. Digital thermocouple

A digital thermocouple[3] is a digital measurement device that measures temperature, displayed in degrees Celsius. The device consists of two conductors of different metals - the hot and the cold junction. When the hot junction is heated, it generates a voltage proportional to the temperature difference between the plates. This measurement is integral to determining the density of the atmosphere inside of the lab.

6. Pressure transducer

The pressure transducer works in a similar way to the absolute pressure transducer described above, but measures the difference between two pressure values, and writes a proportional output in volts. One side of this device reads the stagnation pressure, while the other side reads the static pressure. The measurement obtained from this device is a gauge pressure.

7. Micro-manometer

A micro-manometer[4] is an analog measurement device used to measure pressure, displayed in inches of water. It operates on the principal of hydrostatic equilibrium, which states that the pressure exerted by a column of fluid is proportional to its height and density. The pressure being measured causes a column of water to rise to fall in a clear tube. Once equilibrium is reached and the meniscus is centered between the inscribed lines, a measurement of static gauge pressure drop across the contraction may be taken.

8. Scannivalve

A Scannivalve[5] is a digital measurement device similar to the transducer, and is used to measure pressure at multiple different locations, or 'ports'. It consists of a single transducer and a mechanism that switches the port as needed. This allows for smaller error, as a single machine can read at multiple different points. This measurement provides gauge pressure at several points across the test section.

9. Pitot tube

A pitot tube[6] is a physical tube-shape object with a central hole down the length of the tube and several holes drilled around the outside of the tube. These holes are kept separate, and the pressure transducer is connected across these holes to read the difference, i.e. the dynamic pressure. This is the device connected to the pressure transducer. There is a 90 degree bend present to normalize any disrupting airflow inside the tube.

III. Procedure

A. Data Collection

1. Part 1: Ambient Air Density

For the first part of the data collection, the ambient air density must be determined. This is done by taking measurements of the absolute pressure and the temperature inside the wind tunnel, using the absolute pressure transducer and digital thermocouple, respectively. The governing equation here is the fundamental ideal gas law, Eq.(1), which relates pressure, volume, temperature, matter, and the universal gas constant. This equation can be rearranged and simplified by expanding the term representing matter into m/M, introducing density as $m/\forall$, and defining the specific gas constant as R/M as seen in Eq.(5).

$$p = \frac{m}{\forall}\frac{R}{M}T \tag{5}$$

The result is Eq.(6), which relates pressure, density, and temperature with a known constant value specific to air.

$$p = \rho RT \tag{6}$$

This equation can then rearranged to solve for ρ as a function of p and T, seen in Eq.(7).

$$\rho = \frac{p}{RT} \tag{7}$$

This is the numerical value for density to be used henceforth in this experiment. The error associated with this measurement is found using Eq.(8), derived from Eq.(4), the partial derivatives of Eq.(7) w.r.t. p and T, and the known machine errors, δp and δT.

$$\delta\rho = \sqrt{\left(\frac{1}{RT}\delta p\right)^2 + \left(\frac{p}{RT^2}\delta T\right)^2} \tag{8}$$

2. Part 2: Wind Tunnel Testing

The first step in the process for collecting data for the NACA 0012 airfoil is to measure the chord length, i.e. the distance from the leading to trailing edge along the chord line, and the locations of each pressure tap. These measurements are provided in the airfoil geometry document found on canvas [7].

The next step is to insert the NACA 0012 airfoil into the wind tunnel test section with the leading edge into the free-stream flow. The pressure transducer is connected across the pitot-static tube to measure the dynamic pressure inside the wind tunnel. The Scannivalve ports are connected individually to the pressure taps on the airfoil while the reference port is exposed to ambient pressure. This is to measure test section gauge pressure.

The last step is to run the wind tunnel at a constant fan speed of 40 Hz and record pressure data at each α. The range of angles of attack being tested here are 0, 4, 8, 10, and 12 degrees. This test airfoil has only one set of pressure taps on one side, but considering the symmetry of the airfoil, lower surface data can be recorded on the upper surface by simply testing the airfoil at $\pm\alpha$. Begin by setting the airfoil to $\alpha = -12^\circ$ and recording data at each port 1-9. Set the airfoil to $\alpha = -10^\circ$ and do the same. Repeat this for the rest of the negative and the positive angles of attack. Note $\alpha = 0^\circ$ only needs to be recorded once, as the data will be mirrored across the upper and lower surfaces.

For the NACA 4412 airfoil, the process is very similar. The fan speed is kept constant still at 40 Hz and the range of angles of attack being tested here are 0, 4, 8, 10, and 14 degrees. The test NACA 4412 airfoil has two sets of pressure taps, one set for the upper surface and one set for the lower surface. Connect the scannivalve ports 1-8 across the upper surface pressure taps and record data at *only positive* angles of attack. Then connect the scannivalve ports 1-7 to the lower surface pressure taps and record the pressure data at the same angles of attack.

Using the collected data, the pressure coefficients at each port location across the upper and lower surfaces at each angle of attack can be found. The equation to calculate this can be seen in Eq.(9). Note that the scannivalve readings are reported in units of inches of water and must be converted to pascals for these purposes.

$$C_p = \frac{p_i - p_\infty}{q_\infty}, or, \frac{(Scannivalve)}{(PressureTransducer)} \tag{9}$$

As well as the measured C_p, uncertainty in this value must be calculated. this is done using a modified Eq.(4), Eq.(10) seen below, for the two terms with uncertainty, P_{sv} and P_{td}. The machine error provided in [8] is given in volts and must be converted to pascals. This is done using the conversion factor M found in experiment 1, which converts volts to pascals for both the scannivalve and the pressure transducer.

$$\delta C_p = \sqrt{\left(\frac{\partial C_p}{\partial p_{scv}}\delta p_{scv}\right)^2 + \left(\frac{\partial C_p}{\partial q_\infty}\delta q_\infty\right)^2} \tag{10}$$

The derivation for this error conversion can be seen below. Note that this is an excerpt from the report written on experiment one. This is the conversion factor found for the scannivalve & transducer pressure in volts and pressure in pascals. *Note that the variable E is used for voltage to differentiate it from velocity.*

$$p = ME + b \tag{11}$$

The error associated with this conversion factor can be derived from Eq.(4). Since the data collected is numerical, and Eq.(11) contains only one variable with uncertainty, Eq.(12) is found.

$$\delta p = \sqrt{\sum_{i=0}^{n}\left(\frac{\partial p}{\partial E_i}\delta E_i\right)^2} \tag{12}$$

The caveat here is that the machine error for every measurement taken is the same, allowing this to be simplified greatly, yielding Eq.(13).

$$\delta p = \sqrt{\left(\frac{\partial p}{\partial E}\delta E\right)^2} = \frac{\partial p}{\partial E}\delta E \tag{13}$$

Finally, note that the partial derivative of p w.r.t E is just the conversion factor M, and the final equation for conversion factor error, Eq.(14), is found as a factor of the scannivalve and pressure transducer machine error.

$$\delta p = M\delta E \tag{14}$$

With C_P and δC_p calculated at each pressure tap location across the surfaces of each airfoil for each angle of attack, the coefficients C_x and C_z, as well as the uncertainty associated with these coefficients, δC_x and δC_z, can be calculated using Eq.(15) and Eq.(16) seen below. Note that, as this is a calculation for a dimensionless coefficient, the integration bust be done w.r.t. a dimensionless variable, i.e. $\bar{x}$ and $\bar{z}$. These are defined as the characteristic coordinate divided by the chord length c.

$$C_x = \oint C_p \, d\bar{z}, C_{x_{min}} = \oint C_{p_{min}} \, d\bar{z}, C_{x_{max}} = \oint C_{p_{max}} \, d\bar{z} \tag{15}$$

$$C_z = -\oint C_p \, d\bar{x}, C_{z_{min}} = -\oint C_{p_{min}} \, d\bar{z}, C_{z_{max}} = -\oint C_{p_{max}} \, d\bar{z} \tag{16}$$

Using these values with the specific angle of attack for each airfoil, the coefficients C_l and C_d, as well as the uncertainty associated with these coefficients, δC_l and δC_d, can be calculated using Eq.(17) and Eq.(18) seen below. Note that α is converted into radians for this calculation. Min and max values can be found intuitively using the same equations with C_x min and max and C_z min and max.

$$C_l = C_z \cos\alpha - C_x \sin\alpha; C_{l_{min}} = C_{z_{min}} \cos\alpha - C_{x_{min}} \sin\alpha; C_{l_{max}} = C_{z_{max}} \cos\alpha - C_{x_{max}} \sin\alpha \tag{17}$$

$$C_d = C_x \cos\alpha + C_z \sin\alpha; C_{d_{min}} = C_{x_{min}} \cos\alpha + C_{z_{min}} \sin\alpha; C_{d_{max}} = C_{x_{max}} \cos\alpha + C_{z_{max}} \sin\alpha \tag{18}$$

This C_p data can be plotted in a graph for each airfoil at each angle of attack. The coefficients C_l and C_d can be plotted against α to show the lift and drag slopes as a function of attack angle. On these plots, the ratio of lift to drag, $\frac{L}{D}$ can be plotted as well. The equations for finding lift and drag from the respective coefficients can be seen below in Eq.(19) and Eq.(20). Note that, by the process of division, all terms except for L and D will cancel, and as such $\frac{L}{D}$ is proportional to $\frac{C_l}{C_d}$.

$$L = C_l \cdot q_\infty \cdot c \tag{19}$$

$$D = C_d \cdot q_\infty \cdot c \tag{20}$$

B. Data Processing

1. Part 1: Raw Data Manipulation and Organization

Declare all global variables, including R_{air}, the manometer bias, the provided machine errors, the contraction area ratio, and symbolic variables SC and PT. Define an anonymous function for Eq.(9) using these symbolic variables. Find the dimensionless coordinates for both NACA 0012 and NACA 4412 by dividing the dimensional x-z coordinates by the chord length, seen below in Eq.(21) and Eq.(22). *Be careful to keep units consistent*. To align with the Thin Airfoil Theory, data must be planted at the leading and trailing edge of both airfoils. At the leading edge occurs a stagnation point, where $C_p = 1$, and $\bar{x}$ & $\bar{z}$ are both 0. At the trailing edge, $C_p = 0$, $\bar{x} = 1$, and $\bar{z} = 0$.

$$\bar{x} \equiv \frac{x}{c} \tag{21}$$

$$\bar{z} \equiv \frac{z}{c} \tag{22}$$

Import the data from the 0012 file using `importdata()`, declare a zero matrix with 10 columns, and define a loop to iterate 5 times, once for each angle of attack. Inside the loop, declare dynamic indexing variables, dependent on the current iteration value, to extract the collected data for the upper and lower surface at a single α. *Be sure to take the absolute value of α for the 'lower surface' data, as it was collected and recorded on the upper surface at a negative AoA*. Keeping in mind the standard for closed-loop integration across an airfoil surface, add rows to the 10-column matrix in the following order: trailing edge data plant, lower surface data from ports 9->1, two leading edge data plants, upper surface data from ports 1->9, and another trailing edge data plant. Be sure to add the x-z coordinates corresponding to each port as well. The reasoning for planting two leading edge data points is for sanity when constructing the graphs, and will become clearer later. Careful integration ensures this has no unintended effect on the coefficient calculations.

Next, import the data from the 4412 upper and lower files using `importdata()`, declare a zero matrix with 10 columns, and define a loop to iterate 5 times, once for each angle of attack. Inside the loop, declare dynamic indexing variables, dependent on the current iteration value, to extract the collected data for the upper and lower surface at a single α. Keeping in mind the standard for closed-loop integration across an airfoil surface, add rows to the 10-column matrix

in the following order: trailing edge data plant, lower surface data from ports 7->2, one leading edge data plant, upper surface data from ports 2->8, and another trailing edge data plant. Be sure to add the x-z coordinates corresponding to each port as well.

Extract the individual columns from the full 0012 and 4412 matrices for data processing. Be sure to convert the scannivalve values and machine error values to pascals at this point to prepare to perform the integration. Compute C_p for both airfoils. An anonymous function is not necessarily needed here, but allows for symbolic differentiation and makes error calculations simpler. Compute dq_∞ and dp_{static}, and using Eq.(10), determine the uncertainty across all C_p values.

2. Part 2: Refined Data Calculations

The data processing in part 1 aimed to homogenize the data collected from the two airfoils. The processing at this point forward is pretty much the same for NACA 0012 and NACA 4412, with exceptions for dynamic iteration techniques as a result of the slight differences in port configuration and data configuration. These details will be omitted for the sake of the reader and the author, and specifics on these differences can be found by examining the code in Appendix C. As such, the following process generally describes the steps to be taken for either airfoil geometry.

Begin by initializing matrices to record each α and the corresponding measured, maximum, minimum, and δ values for C_x, C_z, C_l, C_d, and $\frac{L}{D}$. Also divide the length of the full data by the quantity of α to assist with dynamic iteration. Declare a for loop to iterate 5 times. Within, extract the specific C_p, $\bar{x}$, and δC_p. This is a good time to point out that the planted data has no uncertainty, as it is faux and hard-coded to align with the Thin Airfoil Theory. As such, the length of δC_p is dissimilar to the length of C_p across the upper and lower surfaces, and another $\bar{x}$ vector is needed. Using C_p and δC_p, compute the maximum and minimum C_p separately across the upper and lower surfaces. To obtain continuous data for the purposes of plotting, these vectors are homogenized by hard coding the first and last values to the leading and trailing edge pressures. These vectors are then concatenated into single row vectors for plotting. From these values of C_p, $C_{P_{min}}$, and $C_{P_{max}}$, numerical integration is used, specifically `trapz()`, to compute C_x and C_z, as well as the respective max and min values. The ratio $\frac{L}{D}$ is also computed with max and min values. *Inside* the loop, a new figure is configured to plot the entire C_p data for the airfoil at each angle of attack. The x-z cross section is then plotted for sanity.

Finally, on a single figure, C_l, C_d, and the respective uncertainty is plotted as a function of α, corresponding to the left-hand side axis. The ratio $\frac{L}{D}$ is then plotted w.r.t. the right-hand axis.

IV. Results

Raw data used for these calculations can be found in [9–11] The air density inside the wind tunnel was calculated based on the measured temperature T of $31.8°C = 304.95K$[12] and measured p_{atm} of 95.92 kPa, yielding a value of 1.0960 kg/m^3 with an uncertainty of 0.0038 kg/m^3.

Overall, the results show that both the NACA 0012 and the NACA 4412 align with the thin airfoil theory within reason. The thin airfoil theory states that the C_l increases by a value of 0.11 for each 1° increase in α. The graphs of $\frac{C_l}{\alpha}$ for both NACA 0012 and NACA 4412 are shown below in Fig.2 and Fig.3. Looking at how the slopes of these graphs increase as a function of α shows that they fall slightly short of the expected α, but this is to be expected to an extent since the thin airfoil theory is an ideal model, and real-life parameters may differ from ideal models. Note that the maximum C_l for each aerofoil is found at $\alpha = 10°$, according to Fig.2and Fig.3. Also note that the drag is greater overall for NACA 412 then for NACA 0012.

Another interesting point can be seen by analyzing the plot of L/D for both aerofoils. This shows that the 'optimal' AoA, where the maximum lift is produced with the smallest drag, occurs in very different spots. This can be thought of as the 'efficiency' of the aerofoil, and it occurs at a much higher AoA for NACA 0012 than for NACA4412. Thus NACA 4412 can be thought of as being more effective at a lower AoA, as there are less losses due to drag. The specific C_d at each of these peak efficiencies is relatively similar, despite NACA 4412 having overall higher drag.

The results of the C_p vs. c for each aerofoil are within the expected range as well. Knowing a symmetrical airfoil produces no lift at $\alpha = 0°$, the respective graph should have no area between the pressure curves for the upper and lower surfaces. This is in fact the case, as seen in Fig.4. The same is not true for NACA 4412, as it is not symmetrical, and therefore produces lift at $\alpha = 0°$. This can be seen in Fig5. Here, there is an area that results in an upward force being produced on the aerofoil. Some other important results to note are the behaviors of the aerofoils at large angles of attack. at the maximum AoA tested for each aerofoil, the value for C_l drops off and does not continue to follow the expectations under the thin airfoil theory. This can be seen in Fig.2 and Fig.3, as well as in Fig.6 and Fig.7 below: This can be thought of as nearing the stall condition, as if the AoA continues to increase, the C_l will continue to decrease,

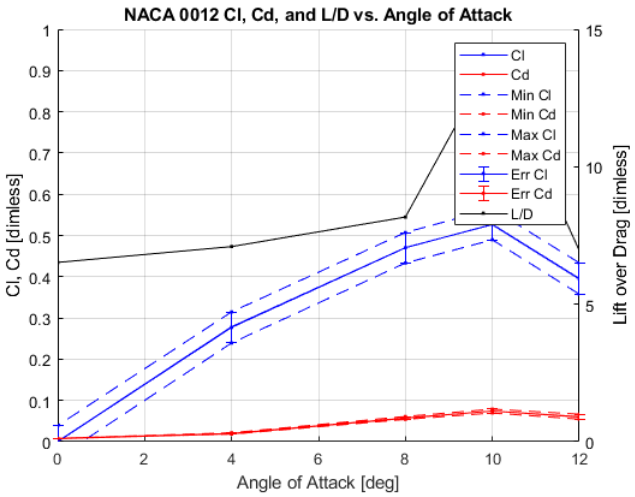

Fig. 2 CAP

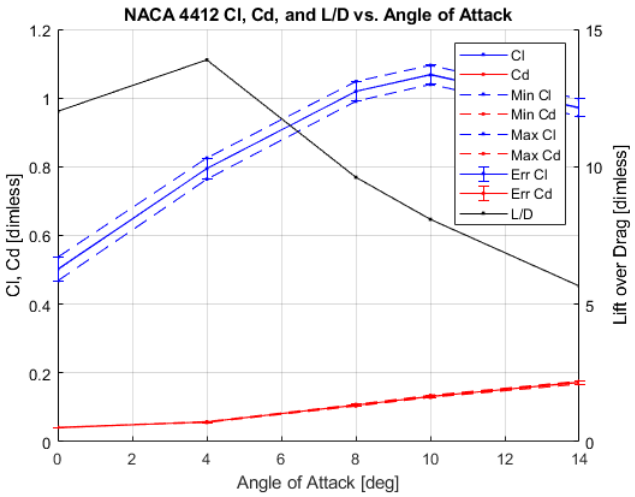

Fig. 3 CAP

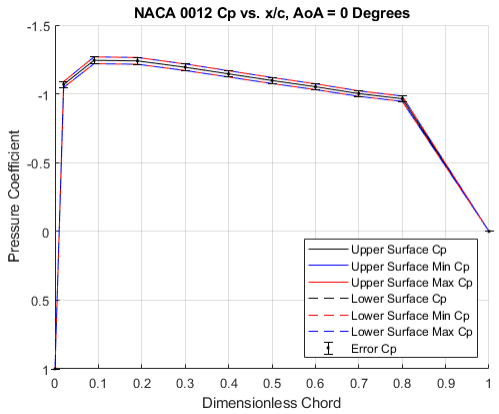

Fig. 4 CAP

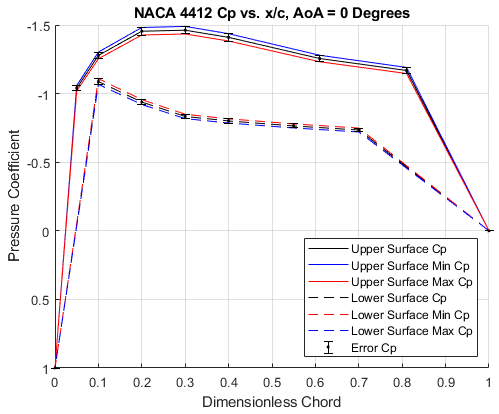

Fig. 5 CAP

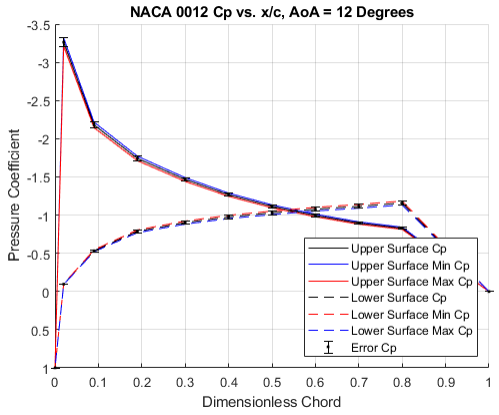

Fig. 6 CAP

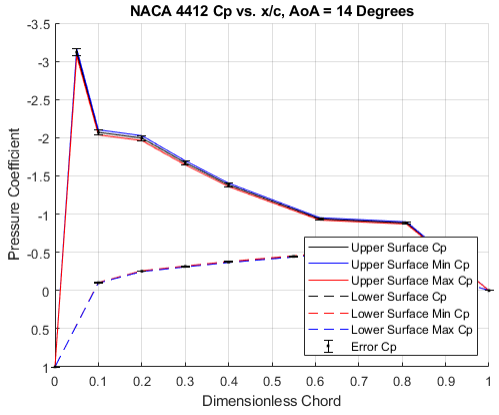

Fig. 7 CAP

and the C_d will continue to increase, eventually causing loss of lift on both aerofoils.

The last thing to note here is the uncertainty in these measurements. Using the machine errors provided and dynamic iteration in code processing, the measured values and curves were plotted with uncertainty on the same figures. Referencing the legend of each graph specifically will provide a more detailed description, but overall it can be seen visually that the maximum and minimum potential values for each calculation are not outside a reasonable range. The

majority of the error lines are within $1-2\%$ of the measured values, and the resulting differences in $\frac{C_l}{\alpha}$ show that the error follows the same slope defined under the thin aerofoil theory, however shifting it by $\pm\delta C_l$. This is generally the case for all uncertainties, but differs slightly in the graphs of C_p vs. c due to the data extrapolation methods.

V. Conclusion

Overall, the experiment successfully met the objective of analyzing the behavior and characteristics of standard aerofoils at varying angles of attack. Using the calibrated measurement instruments and the density of lab air, pressures could be recorded at various locations on each aerofoil at differing angles of attack. While the method varied depending on which aerofoil was being tested, the data was able to be manipulated and homogenized in a way to make it presentable for analysis. The assumptions made prior to experimentation are crucial to obtaining any sort of meaningful calibration. They allow for a simpler derivation of pressure and velocity using physical laws like the conservation of mass and Bernoulli's equation, which may not apply without these working assumptions. The results of the previous experiment show that these assumptions had next to no negative affect on the measurements, as each instrument measures the pressure and velocity with great accuracy in comparison to the true velocity. These measured pressures, proven accurate within an acceptable range, were then used to determine the behavior of these aerofoils in steady flow within an acceptable range. The overall error and uncertainty in this experiment was found to be very small. All values lie within an acceptable range, as described above in the results. This further speaks to the validity of the assumptions made, and should incite confidence in the measurement tools used and the accuracy of the measured results. Some potential sources of error are, of course, the known machine error. Aside from this, Other sources include the human error in setting the angle of attack, since it was done using a protractor attached to the aerofoil. This is completely down to human accuracy, which could introduce some uncertainty. Rounding error is unlikely, since the computations were performed using computer software. The results of the experiment show us that, while the rate of lift increase for both aerofoils, NACA 4412 produces lift at a zero AoA, unlike NACA 0012. It is also more efficient at lower angles of attack, producing more lift with less drag at a lower AoA. It does produce more drag overall though, especially at a higher AoA. NACA 0012 and NACA 4412 both achieve peak lift at an AoA of roughly $10°$. NACA 4412 should maintain lift for a wider range of AoA, as the downward trend seen after $\alpha = 10°$ begins from a higher C_l, and should take 'longer' to reach 0. Overall, it seems as though the NACA 4412 is a better choice, but this is application dependent of course.

VI. Acknowledgements

I would first like to thank my lab TA for the beautiful figures and guidance throughout the experiment. I would also like to thank Monster Beverage Corporation for providing me with the necessary caffeine to get through this week. Lastly I would like to thank my cat Robby for the moral support he provided, i.e. screaming outside my door whenever I did not let him watch me do my homework and step on my keyboard.

References

[1] NASA, "Low speed tunnel operation," , 2021. URL https://www.grc.nasa.gov/www/k-12/airplane/tunop.html.

[2] Craig, B., "What is absolute pressure transmitter [and] how does it work?" , Jul 2023. URL https://www.transmittershop.com/blog/absolute-pressure-transmitter-working-principle-applications/#:~:text=Simply%2C%20the%20side%20of%20the,mechanical%20energy%20into%20electrical%20signals.

[3] munroscientificdivision, 2024. URL https://www.munroscientific.co.uk/a-guide-for-laboratory-thermometer#:~:text=A%20laboratory%20thermometer%20is%20an,scale%20that%20indicates%20the%20temperature.

[4] click2electro, "Manometer Basics & Micromanometer," , Apr 2023. URL https://click2electro.com/forum/instrumentation-measurement/manometer-basics-micromanometer/.

[5] links open overlay panelGiuseppe P. Russo, A., and chapter highlights pressure sensors ranging from the classical manometers, A., "Pressure sensors," , Mar 2014. URL https://www.sciencedirect.com/science/article/pii/B9781845699925500012.

[6] NASA, "Pitot tube," , 2024. URL https://www.grc.nasa.gov/www/k-12/VirtualAero/BottleRocket/airplane/pitot.html.

[7] AEE361, "AEE360LAB2AirfoilGeometry," , 2024. URL https://canvas.asu.edu/courses/200674/files/92667501?module_item_id=14753583.

[8] AEE361, "Machine error chart.xls," , 2024. URL https://canvas.asu.edu/courses/200674/files/90845854?module_item_id=14598811.

[9] ThuB600, "Lab2_ThuB600_0012.txt," , 2024. URL https://canvas.asu.edu/courses/200674/files/93778685?module_item_id=14821802.

[10] ThuB600, "Lab2_ThuB600_4412U.txt," , 2024. URL https://canvas.asu.edu/courses/200674/files/93778681?module_item_id=14821800.

[11] ThuB600, "Lab2_ThuB600_4412L.txt," , 2024. URL https://canvas.asu.edu/courses/200674/files/93778683?module_item_id=14821801.

[12] CalculatorSoup, L., "Celsius to Kelvin: °C to K," , Aug 2023. URL https://www.calculatorsoup.com/calculators/conversions/celsius-to-kelvin.php.